Surface characteristics, mechanical properties, and cytocompatibility of oxygen plasma-implanted porous nickel titanium shape memory alloy

S.L. Wu,[1] Paul K. Chu,[1] X.M. Liu,[1] C.Y. Chung,[1] J.P.Y. Ho,[1] C.L. Chu,[1,2] S.C. Tjong,[1] K.W.K. Yeung,[3] W.W. Lu,[3] K.M.C. Cheung,[3] K.D.K. Luk[3]

[1]*Department of Physics and Materials Science, City University of Hong Kong, Tat Chee Avenue, Kowloon, Hong Kong*
[2]*Department of Materials Science and Engineering, Southeast University, Nanjing, People's Republic of China*
[3]*Division of Spine Surgery, Department of Orthopaedics and Traumatology, The University of Hong Kong, Pokfulam, Hong Kong*

Received 23 November 2005; accepted 22 December 2005
Published online 15 June 2006 in Wiley InterScience (www.interscience.wiley.com). DOI: 10.1002/jbm.a.30705

Abstract: Good surface properties and biocompatibility are crucial to porous NiTi shape memory alloys (SMA) used in medical implants, as possible nickel release from porous NiTi may cause deleterious effects in the human body. In this work, oxygen plasma immersion ion implantation (O-PIII) was used to reduce the amount of nickel leached from porous NiTi alloys with a porosity of 42% prepared by capsule-free hot isostatic pressing. The mechanical properties, surface properties, and biocompatibility were studied by compression tests, X-ray photoelectron spectroscopy (XPS), and cell culturing. The O-PIII porous NiTi SMAs have good mechanical properties and excellent superelasticity, and the amount of nickel leached from the O-PIII porous NiTi is much less than that from the untreated samples. XPS results indicate that a nickel-depleted surface layer predominantly composed of TiO_2 is produced by O-PIII and acts as a barrier against out-diffusion of nickel. The cell culturing tests reveal that both the O-PIII and untreated porous NiTi alloys have good biocompatibility. © 2006 Wiley Periodicals, Inc. J Biomed Mater Res 79A: 139–146, 2006

Key words: porous nickel–titanium; shape memory alloys; plasma immersion ion implantation; biocompatibility

INTRODUCTION

Nickel–titanium (NiTi) shape memory alloys (SMA) have attracted much attention because of their unique shape memory effect and superelasticity.[1–3] These functional characteristics combined with good biocompatibility make NiTi alloys useful in biomedical applications.[4,5] However, their higher Young's modulus (about 80 GPa for austenite[4]) when compared with that of human bone, either cancellous (1–2 GPa) or compact bones (17.0–18.9 GPa),[6,7] restricts the use of dense NiTi in some applications. Porous NiTi alloys have recently been developed and emerged to be one of the promising biomaterials for surgical implants. Because of the interconnected open pores and large surface area, transport of body fluids and in-growth of bone tissues are possible with this unique material.[8–10]

The manufacturing processes and characterization of porous NiTi SMAs have been reported. Chu et al.[11] produced porous NiTi SMAs by combustion synthesis, but the stress–strain curve obtained in their work did not exhibit an obvious stress plateau and the materials were brittle and fractured at a stress of about 200 MPa. The porous NiTi SMAs prepared by Li et al.[12] using powder sintering also showed no stress plateau in the stress–strain curve. Kim et al. [13] fabricated porous NiTi SMAs by using self-propagating high temperature synthesis, but the materials still had a brittle nature. Therefore, it is necessary to develop a new method to manufacture porous NiTi SMAs with higher ductility as well as adjustable porous structure. Yuan et al.[14] have recently fabricated porous NiTi SMAs by the capsule-free hot isostatic pressing (CF-HIP) method. The materials exhibit isotropic and uniform pore distribution as well as good mechanical properties. CF-HIP, which is quite different from traditional HIP, has been used to improve the mechanical properties of ceramic materials while retaining ade-

Correspondence to: P.K. Chu; e-mail: paul.chu@cityu.edu.hk
Contract grant sponsor: Hong Kong Research Grants Council (RGC) Central Allocation Group Research; contract grant number: CityU 1/04C.

quate porosity in the as-pressed powders, because the high gas pressure prevents densification and enhances bridging between particles. In addition, this method also reduces the formation of micro-cracks and closed pores.[15,16] In this work, we adopted CF-HIP to produce the porous NiTi SMAs.

It is well known that nickel ions released from nickel-containing alloys is one of the common causes for allergic contact dermatitis.[17] The corrosion resistance of NiTi and toxicity of the by-products released from corroded surfaces have been studied.[18,19] A surface barrier layer such as titanium oxide, titanium nitride, or titanium carbide has been shown to improve the wear resistance, corrosion resistance, and biocompatibility of dense NiTi SMAs.[20–24] Compared to conventional dense NiTi, the complex surface morphology and large surface areas of porous NiTi pose a more serious problem with regard to Ni release. The demand on the surface modification technique is thus more stringent. Plasma immersion ion implantation (PIII), which excels as a non-line-of-sight technique, has been demonstrated on components with irregular geometries.[24–27] In addition, a good theoretical understanding of PIII into complex-shaped samples such as industrial gears and ball bearings has been developed and simulation software is available to determine ion trajectories and ion fluence distributions along various types of surfaces.[28–31] PIII has been successfully used to improve the surface mechanical and biological properties of dense NiTi SMAs,[32–34] and in this work, we investigated the use of oxygen PIII to enhance the surface properties of porous NiTi SMA made by CF-HIP. We studied the surface characteristics, compression strength, nickel release behavior, as well as cultured cell behavior on the plasma-treated porous NiTi SMAs.

MATERIALS AND METHODS

Preparation of materials

Superelastic porous NiTi SMAs with a porosity of 42% were fabricated with equiatomic nickel powders and titanium powders (NI006021 Nickel, Goodfellow Corporation; Titanium, Shanghai Reagent Corporation) by CF-HIP using a capsule-free HIP unit (ABB Company). The starting materials were placed in the HIP chamber and the temperature and argon pressure were simultaneously raised to 1050°C and 150 MPa, respectively and kept for 3 h. Finally, the temperature and argon pressure were gradually reduced allowing the pores filled with compressed argon to expand resulting in the formation of a porous structure. The samples used for cell culture and surface analysis were machined into disks 5 mm in diameter and 2 mm thick. Before PIII, the plates were mechanically polished by sandpapers, ultrasonically cleaned with acetone, and then oven-dried. The surface morphology of the samples was evaluated by scanning electron microscopy (SEM-JSM5200)

TABLE I
Oxygen Plasma Immersion Ion Implantation Parameters

RF Power	1000 W
Sample Voltage	40 kV
Pulse Width	50 μs
Frequency	200 Hz
Pulse Duration	120 min
Base Pressure	1×10^{-5} Torr
O_2 Working Pressure	6.0×10^{-4} Torr

Oxygen plasma immersion ion implantation

Before oxygen PIII, the surface of the porous NiTi samples was cleaned using argon plasma for 5 min. Oxygen PIII was then carried out using the parameters listed in Table I on both sides of the samples. The details of the PIII instrument can be found elsewhere.[35,36]

Compression test

Porous NiTi bars 12 mm in length and 6 mm in diameter were used in our mechanical tests. Before the compression test, the bars were treated by oxygen plasma immersion ion implantation (O-PIII) (Table I). Uniaxial compression tests were carried out at a constant rate of 0.06 mm/min at a room temperature of about 22°C using an Instron 4206.

Surface analysis

The surface structure of the O-PIII samples was characterized by X-ray photoelectron spectroscopy (XPS) (Physical electronics PHI 5802, MN) using an aluminum X-ray source with a power of 350 W, a pass energy of 11.75 eV for narrow scans, and an analysis area ~0.8 mm^2 at a vacuum of 2×10^{-8} Pa. Survey scans were first obtained to identify the atomic species on the surfaces from a binding energy range of 0–1400 eV using a pass energy of 187.85 eV. A take-off angle of 45° was used in all sample analysis. The binding energies were calibrated using the C1s peak at 284.6 eV. A Gaussian-Lorentzian peak fitting model was used to deconvolute the Ti2p spectra.

Immersion tests

In the simulated body fluid (SBF) immersion test, three lots (three samples per lot) were used for both the untreated and O-PIII porous NiTi samples. Each sample was separately immersed in 25 mL of the SBF solution at 37 ± 0.5°C. The composition of the SBF is shown in Table II. After 70 days, the released nickel concentrations in the SBF were

TABLE II
Chemical Compositions of SBF (g/L)

NaCl	7.996
$NaHCO_3$	0.350
KCl	0.224
$K_2HPO_4 \cdot 3H_2O$	0.228
$MgCl_2 \cdot 6H_2O$	0.305
$CaCl_2$	0.278
Na_2SO_4	0.071
$(CH_2OH)_3CNH_2$	6.057

measured using inductively-coupled plasma mass spectrometry (ICPMS) (Perkin Elmer, PE SCIEX ELAN6100, USA).

Cell cultures

To investigate the cytocompatibility of the plasma-treated and untreated samples, osteoblasts isolated from calvarial bones of 2-day-old mice that ubiquitously expressed an enhanced green fluorescent protein (EGFP) were cultured in a Dulbecco's Modified Eagle Medium (Invitrogen) supplemented with 10% (v/v) fetal bovine serum (Biowest, France), antibiotics (100 U/mL of penicillin and 100 μg/mL of streptomycin), and 2 m*M* L-glutamine at 37°C in an atmosphere of 5% CO_2 and 95% air. The specimens (1 mm thick and 5 mm in diameter) were fixed onto the bottom of a 24-well tissue culture plate (Falcon) using 1% (w/v) agarose. A cell suspension consisting of 5000 cells was seeded onto the surface of the untreated porous NiTi samples, the O-PIII porous NiTi samples, and wells without any metal discs serving as a control for normal culturing conditions. Cells were grown in 1 mL of medium and changed every 3 days. Five identical samples were used. The cell proliferation was examined after 8 days of culture. In this study, the cells were allowed to reach confluence during the examination period.

The attached living EGFP-expressing osteoblasts were visualized using a fluorescent microscope (Axioplan 2, Carl Zeiss, Germany) with a 450–490 nm incident filter and the fluorescence images emitted at 510 nm captured using a Sony DKS-ST5 digital camera.

RESULTS

Surface characteristics of O-PIII porous NiTi alloys

Figure 1 shows the microstructure of the porous NiTi samples made by CF-HIP. The size of most of interconnecting pores varies from about 50 to 400 μm, which falls in the conventional range of 50–500 μm suitable for tissue integration.[37] The small pores are interconnected with big pores [shown by the arrows in the Fig. 1(b)]. The typical XPS survey spectra acquired from the untreated and oxygen plasma-implanted porous NiTi samples are shown in Figures 2(a,b). The presence of argon is due to surface cleaning by argon sputtering. The trace amounts of carbon and nitrogen possibly come from surface contamination. It can be observed that the Ni2p peak intensity is sharply lower and the oxygen peak intensity is significantly higher in the O-PIII porous NiTi sample. Figure 3 shows the XPS depth profiles of the untreated and plasma-implanted porous NiTi samples. The profiles have been plotted on a depth scale using a sputtering rate of 17.45 nm/min derived from a SiO_2 reference under similar conditions. The depth profiles show the presence of a very thin (about 10 nm thick) nickel depleted layer on the surface of the untreated porous sample [between lines a and b, shown in Fig. 3(a)], whereas that on the O-PIII porous NiTi is about 70 nm thick as demarcated by lines a and b in Figure 3(b). The nickel concentration of O-PIII porous NiTi gradually increases between lines b and c, but is still below that of titanium. The thickness of this transition layer is about 28 nm. Beneath this layer, there is a zone in which the Ni concentration is slightly higher than that in the

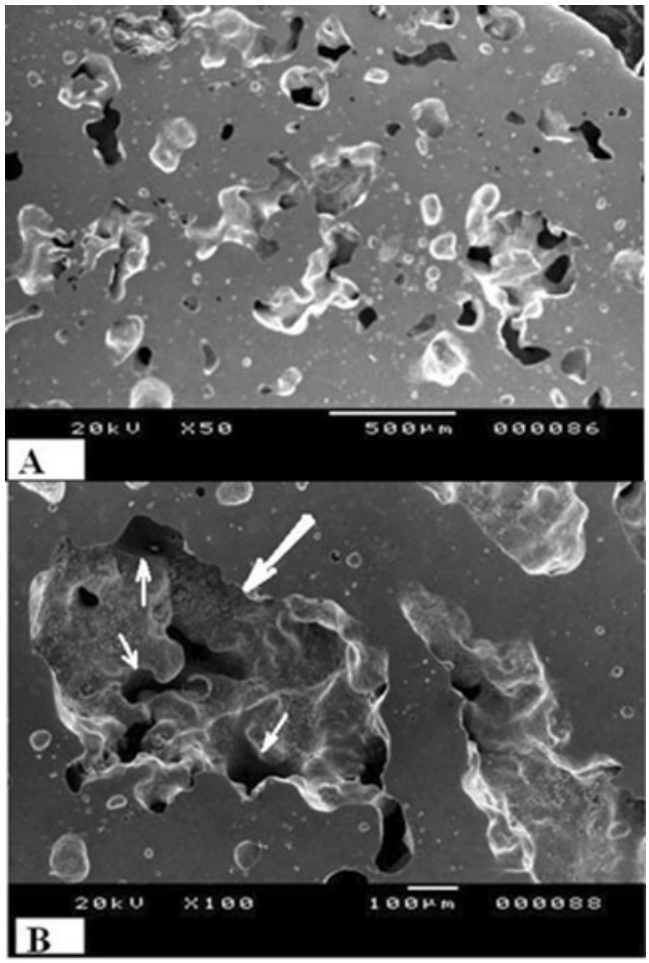

Figure 1. Microstructures of porous NiTi sample prepared by CF-HIP: (a) SEM image of porous sample; (b) high magnification detail of (a).

bulk materials [demarcated by lines d and e in Fig. 3(b)]. At a greater depth [beneath line e, shown in Fig. 3(b)], the Ni concentration reverts back to the value of the bulk materials of about 50%.

Figure 4 shows the XPS spectra and corresponding fitted peaks of Ti2p and Ni2p of the untreated and O-PIII porous NiTi samples at different depths. As shown in Figure 4(a), the measured binding energy of $Ti2p_{3/2}$ on the ion implanted surface is 458.9 eV and the difference in the binding energy between $Ti2p_{1/2}$ and $Ti2p_{3/2}$, △, is 5.5 eV. The results, which are consistent with the reported values in TiO_2,[38,39] reveal that Ti exists only as TiO_2 on the surface of O-PIII sample, although three chemical states of Ti can be observed on the surface of the untreated sample, namely, Ti^0 (NiTi), Ti^{2+} (TiO), and Ti^{4+} (TiO_2), [shown in Fig. 4(b)]. With regard to Ni, according to the reported binding energies,[39] it can be found from Figure 4(d) that only metallic Ni^0 (NiTi) exists on the surface of the untreated sample (852.9 eV binding energy for $Ni2p_{3/2}$ and 17.3 eV for △, binding energy difference

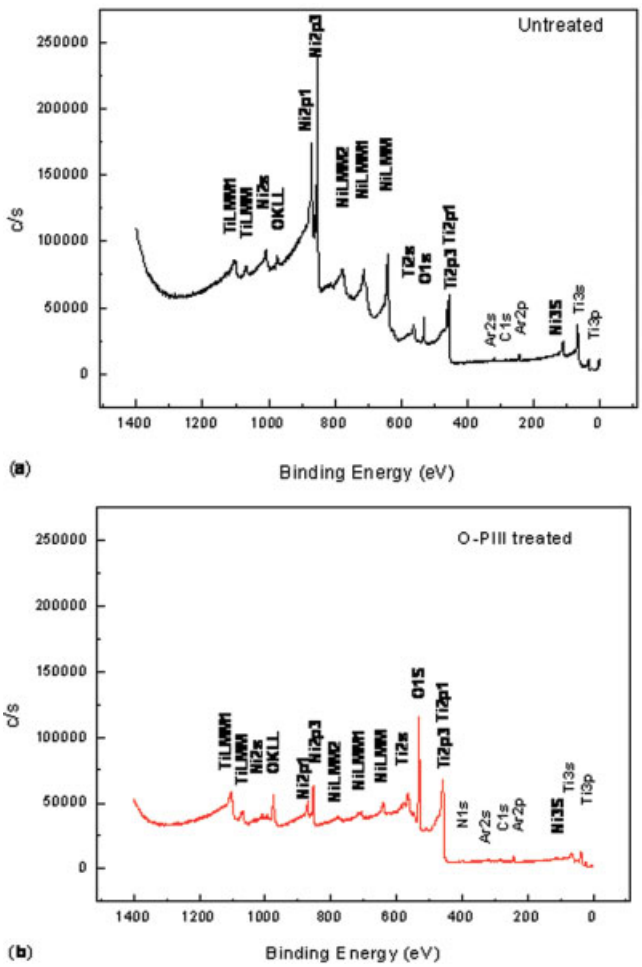

Figure 2. XPS survey scan spectra of the porous NiTi samples; (a) Untreated, (b) O-PIII treated. [Color figure can be viewed in the online issue, which is available at www.interscience.wiley.com.]

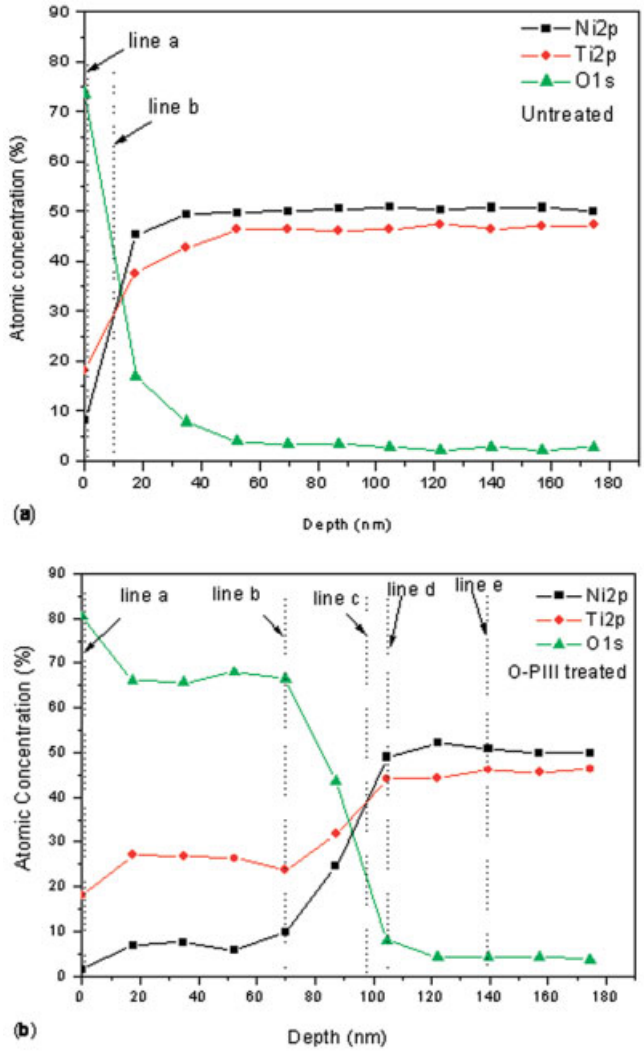

Figure 3. XPS depth profile of porous NiTi samples; (a) Untreated, (b) O-PIII treated. [Color figure can be viewed in the online issue, which is available at www.interscience.wiley.com.]

between $Ni2p_{1/2}$ and $Ni2p_{3/2}$). For the O-PIII sample, the measured binding energy of $Ni2p_{3/2}$ is 854.1 eV, corresponding to Ni^{2+} (NiO), implying that trace amounts of NiO are formed on the surface during O-PIII [shown in Fig. 4(c)]. To obtain information at different depths, XPS was performed after 4 min of sputtering with argon to remove about 70 nm of materials. At this depth, in the O-PIII porous NiTi sample, besides large amounts of TiO_2, Ti_2O_3, TiO, and a trace amount of NiTi are detected. In the untreated porous NiTi sample, TiO_2 can no longer be detected at this depth and large amounts of NiTi and trace amounts of Ti_2O_3 and TiO exist. After further sputtering of the O-PIII sample for 10 min to remove about 170 nm of materials, large amounts of NiTi are observed and only trace amounts of TiO and Ti_2O_3 can be detected at this depth.

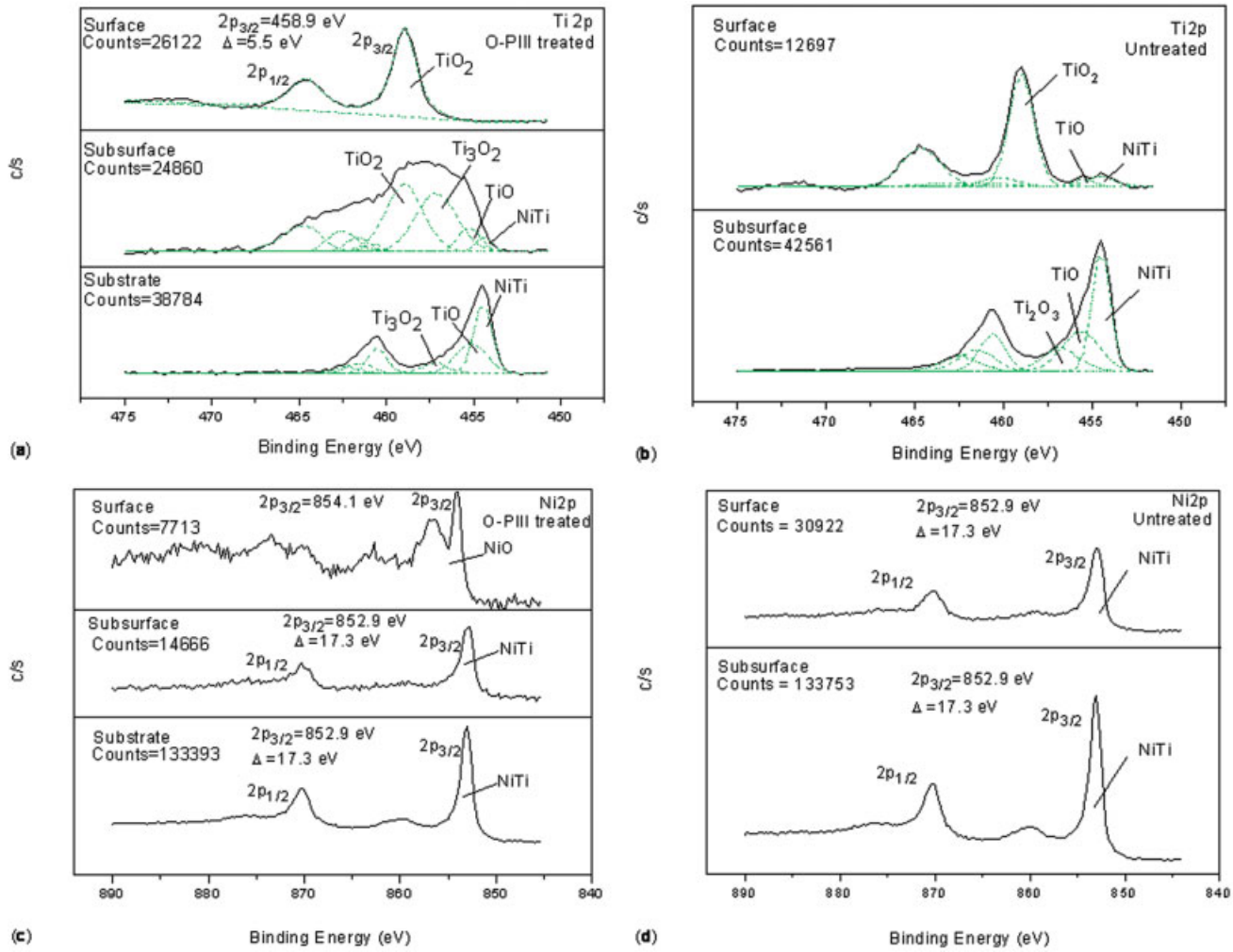

Figure 4. XPS spectra of Ti2p and Ni2p acquired from the untreated and O-PIII porous NiTi samples. The solid line (black color) indicates the experimental spectra and the dash dot line (green color) indicates the fitted spectra. (a) Ti2p from O-PIII sample; (b) Ti2p from untreated sample; (c) Ni2p from O-PIII sample; (d) Ni2p from untreated sample. [Color figure can be viewed in the online issue, which is available at www.interscience.wiley.com.]

Mechanical properties

Figure 5 shows the compressive stress–strain results of the untreated and O-PIII porous NiTi bars strained up to 4.7%. The compressive strength of the untreated and O-PIII porous NiTi SMAs is about 330 and 300 MPa, respectively, when strained up to 4.7%. In addition, the width of the hysteretic loop of the two curves is quite small, and the remaining strain in the untreated and O-PIII samples is only about 0.042 and 0.053%, respectively, when the unloading process is completed.

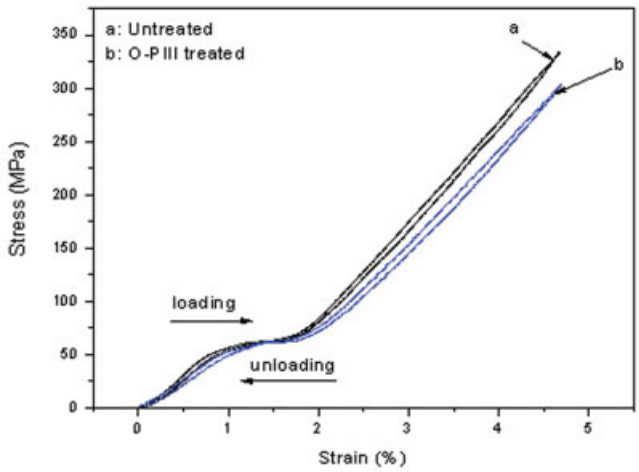

Figure 5. Stress versus strain diagrams of porous NiTi alloys. The black line indicates the untreated sample and the blue line indicates O-PIII-treated sample. [Color figure can be viewed in the online issue, which is available at www.interscience.wiley.com.]

Assessment of nickel release and cytocompatibility

Figure 6 shows the released nickel concentrations after SBF immersion at 37°C for 70 days. The amount

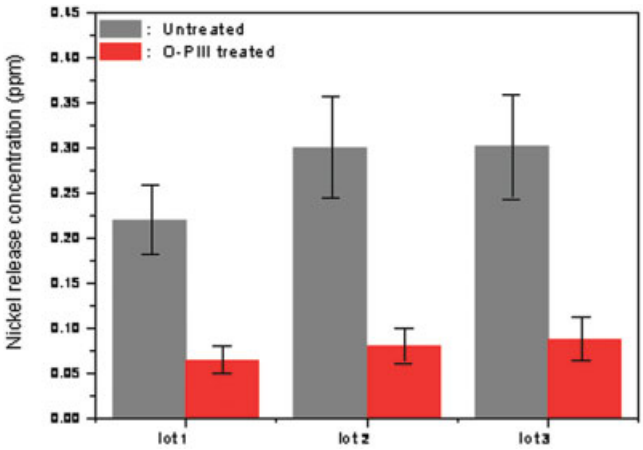

Figure 6. Amount of nickel released from the porous NiTi samples immersed in SBF at 37 ± 0.5°C for 70 days determined by ICPMS. [Color figure can be viewed in the online issue, which is available at www.interscience.wiley.com.]

of leached nickel from all porous samples is observed to be significantly mitigated after oxygen PIII. Figure 7(a,b) shows the results of cell proliferation on the untreated and O-PIII porous samples after 8 days of culture. Both the O-PIII and untreated samples are well tolerated by the EGFP-expressing osteoblasts. The cells clearly attach to and proliferate on the samples, indicating that at least in our short term *in vitro* test, no immediate cytotoxic effects can be seen. We are currently performing more long term *in vitro* as well as *in vivo* test to assess the longer term viability of the plasma-treated porous materials.

DISCUSSION

The formation of TiO_2 and TiO on the untreated porous NiTi sample is due to natural oxidation of Ti during mechanical polishing as well as exposure to air. Since the concealed surfaces are more difficult to oxidize and mechanical polishing cannot reach most of the pores, only a thickness of about 10 nm with depleted Ni can be found on the surface of the untreated sample and the metallic Ni (NiTi) concentration increases from about 8 at.% to about 28 at.% after this surface layer. The Ni concentration gradually reaches about 50% at a larger depth corresponding to the Ni content in the bulk of the materials. Formation of trace amounts of TiO and Ti_2O_3 is possibly due to oxidation of the Ti powders during CF-HIP. The surface of the O-PIII sample is predominantly composed of TiO_2 and a trace amount of NiO. It is a stable oxide layer composed of TiO_2, Ti_2O_3, TiO, and a trace amount of NiTi. A transition layer exists beneath this surface layer because of the roughly Gaussian distribution of the implanted ions. The occurrence of a Ni-rich zone [shown by lines d and e in Fig. 3(b)] can be explained by the mechanism proposed by Tietze et al.[40] Excess oxygen on the implanted surface leads to Ti diffusion from the bulk to form TiO_2 leaving a Ni-rich zone in this transition region.

Unlike the porous NiTi prepared by other methods,[11–13] both the untreated (mechanically polished) and O-PIII porous bars exhibit an obvious stress plateau similar to that of dense NiTi. It means that after reaching a critical stress of about 50 MPa, the porous NiTi samples start to transform into martensite. Upon further straining, the stress is almost constant until the porous samples are fully transformed. The reverse transformation occurs during unloading, indicating a stress-induced transformation in the porous NiTi SMAs produced by CF-HIP during loading or unloading. Our data reveal that both the untreated and O-PIII porous NiTi SMAs have good mechanical properties and excellent super-elasticity, and O-PIII has little ef-

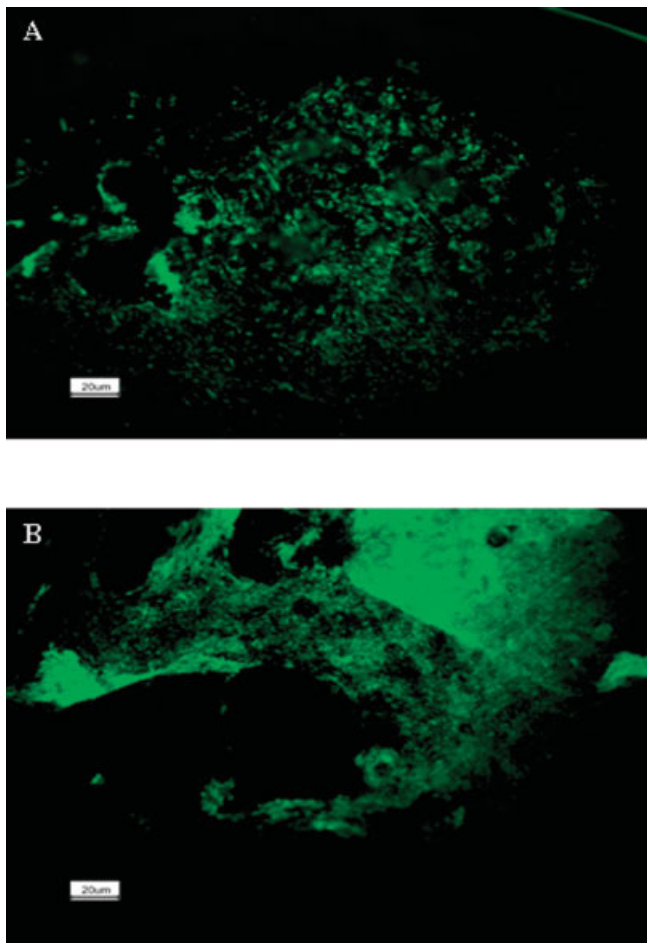

Figure 7. Microscopic view of porous NiTi alloy with or without implantation after 8 days of cell culturing showing the EGFP-expressing mouse osteoblasts. Proliferation clusters are obviously seen on the surface (×4 magnifications) of: (a) porous NiTi without implantation and (b) O-PIII sample. [Color figure can be viewed in the online issue, which is available at www.interscience.wiley.com.]

fects on the mechanical properties of porous NiTi alloys.

The ICPMS results unequivocally indicate that oxygen PIII can prevent the leaching of Ni ions from the porous sample, when compared with other techniques, which may have difficulty dealing with nonplanar surfaces. In this work, the untreated (mechanically polished) sample shows higher nickel release, probably due to the thinner oxide layer on the surface. Another important factor is that the surface of the pores cannot be oxidized during mechanical polishing, whereas these pores are more effectively implanted during PIII. For pores with a size of 50–400 μm, they are sufficiently big that the plasma can penetrate into them and so the sidewalls can be adequately implanted, as PIII has been shown to implant the sidewalls of sub-micrometer trench structures in integrated circuits having aspect ratios exceeding 30.[41] However, we are not implying that all the sidewalls of the pores have been adequately implanted during PIII, as small and deep pores are still difficult to implant. Nonetheless, our immersion tests reveal unambiguous improvement offered by O-PIII. We are conducting more work to further optimize the PIII process. It should also be noted that while O-PIII yields a number of advantages such as mitigation in Ni leaching, no deleterious effects on either the mechanical and biological properties have been noticed as described earlier.

CONCLUSIONS

Porous NiTi SMAs produced by capsule-free method (CF-HIP) are modified by O-PIII. Our SBF immersion tests reveal that oxygen PIII can significantly reduce the release of Ni from the porous materials. The improvement can be attributed to the formation of a stable surface layer predominantly composed of TiO_2 and trace amounts of NiO. The compression test reveals that both the untreated and O-PIII porous NiTi alloys have good mechanical properties and excellent super-elasticity. The cell culturing results indicate that both the O-PIII and untreated porous NiTi have good cytocompatibility. Therefore, O-PIII offers many advantages such as reduction in Ni leaching but does not introduce any deleterious mechanical and biological effects.

References

1. Buehler WJ, Wang FE. A summary of recent research on the nitinol alloys and their potential application in ocean engineering. Ocean Eng 1968;1:105–108.
2. Stachowiak GB, McCormick PG. Shape memory behavior associated with the R and martensitic transformations in a NiTi alloy. Acta Metall 1988;36:291–297.
3. Wever DJ, Veldhuizen AG, Sanders MM, Schakenraad JM, Van Horn JR. Cytotoxic, allergic and genotoxic activity of a nickel-titanium alloy. Biomaterials 1997;18:1115–1120.
4. Helsen JA, Jurgen Breme H. Metals as Biomaterials. New York: Wiley; 1998. p 80–97.
5. Bogdanski D, Koller M, Muller D, Muhr G, Bram M, Buchkremer HP, Stover D, Choi J, Epple M. Easy assessment of the biocompatibility of Ni-Ti alloys by in vitro cell culture experiments on a functionally graded Ni-NiTi-Ti material. Biomaterials 2002;23:4549–4555.
6. Gibson LJ. The mechanical behavior of cancellous bone. J Biomech 1985;18:317–328.
7. Suchanek W, Yoshimura M. Processing and properties of hydroxyapatite-based biomaterials for use as hard tissue replacement implants. J Mater Res 1998;13:94–117.
8. Simske SJ, Sachdeva R. Cranial bone apposition and ingrowth in a porous nickel-titanium implant. J Biomed Mater Res 1995; 29:527–533.
9. Ayers RA, Simske SJ, Bateman TA, Petkus A, Sachdeva RLC, Gyunter VE. Effect of nitinol implant porosity on cranial bone ingrowth and apposition after 6 weeks. J Biomed Mater Res 1999;45:42–47.
10. Itin VI, Gyunter VE, Shabalovskaya SA, Sachdeva RLC. Mechanical properties and shape memory of porous nitinol. Mater Charact 1994;32:179–187.
11. Chu CL, Chung CY, Lin PH, Wang SD. Fabrication of porous NiTi shape memory alloy for hard tissue implants by combustion synthesis. Mater Sci Eng A 2004;366:114–119.
12. Li BY, Rong LJ, Li YY. Stress-strain behavior of porous Ni-Ti shape memory intermetallics synthesized from powder sintering. Intermetallics 2000;8:643–646.
13. Kim JS, Yang SG, Kang JH, Kang SB, Yoon KS, Kwon YS. Porous TiNi biomaterial produced by self-propagating high-temperature synthesis: Pore structure, mechanical property and application. Mater Sci Forum 2004;449:1097–1100.
14. Yuan B, Chung CY, Zhu M. Microstructure and martensitic transformation behavior of porous NiTi shape memory alloy prepared by hot isostatic pressing processing. Mater Sci Eng A 2004;382:181–187.
15. Hayashi T, Sugihara S, Okazaki K. Preparation of porous PZT with high connectivity using capsule-free O_2-HIP and their dielectric-properties. Ferroelectrics 1992;131:75–82.
16. Tamai M, Miki S, Pezzotti G, Nakahira A. Fabrication and evaluation of porous hydroxyapatite by pressureless sintering and capsule-free HIP sintering. J Ceram Soc Jpn 2000;108:915–920.
17. Blancodalmau L, Carrasquilloalberty Dalmau H, Silvaparra J. A study of nickel allergy. J Prosthet Dent 1984;52:116–119.
18. Shih CC, Lin SJ, Chen YL, Su YY, Lai ST, Wu GJ, Kwok CF, Chung KH. The cytotoxicity of corrosion products of nitinol stent wire on cultured smooth muscle cells. J Biomed Mater Res 2000;52:395–403.
19. Heintz C, Riepe G, Birken L, Kaiser E, Chakfe N, Morlock M, Delling G, Imig H. Corroded nitinol wires in explanted aortic endografts: An important mechanism of failure? J Endovasc Ther 2001;8:248–253.
20. Wang DY, Chiu MC. Characterization of TiN coatings post-treated by metal-plasma ion implantation process. Surf Coat Technol 2002;156:201–207.
21. Trepanier C, Tabrizian M, Yahia L, Bilodeau L, Piron DL. Effect of modification of oxide layer on NiTi stent corrosion resistance. J Biomed Mater Res 1998;43:433–440.
22. Kao CT, Ding SJ, Chen YC, Huang TH. The anticorrosion ability of titanium nitride (TiN) plating on an orthodontic

metal bracket and its biocompatibility. J Biomed Mater Res 2002;63:786–792.
23. Cisse O, Savadogo O, Wu M, Yahia L. Effect of surface treatment of NiTi alloy on its corrosion behavior in Hanks' solution. J Biomed Mater Res 2002;61:339–345.
24. Liu XY, Chu PK, Ding CX. Surface modification of titanium, titanium alloys, and related materials for biomedical applications. Mater Sci Eng R Rep 2004;47:49–121.
25. Chu PK, Qin S, Chan C, Cheung NW, Larson LA. Plasma immersion ion implantation—A fledgling technique for semiconductor processing. Mater Sci Eng R Rep 1996;17:207–280.
26. Zeng XC, Kwok TK, Liu AG, Chu PK, Tang BY, Sheridan TE. Effects of the auxiliary electrode radius during plasma immersion ion implantation of a small cylindrical bore. Appl Phys Lett 1997;71:1035–1037.
27. Zeng ZM, Chu PK, Tian XB, Tang BY, Kwok TK. Ion implantation into race surfaces of aerospace ball bearings in a plasma immersion configuration. IEEE Trans Plasma Sci 2000;28:394–402.
28. Sheridan TE, Kwok TK, Chu PK. Kinetic model for plasma-based ion implantation of a short, cylindrical tube with auxiliary electrode. Appl Phys Lett 1998;72:1826–1828.
29. Zeng ZM, Kwok TK, Tian XB, Tang BY, Chu PK. Investigation of dose uniformity on the inner races of bearings treated by plasma immersion ion implantation. J Appl Phys 1999;86:120–123.
30. Wood BP, Rej DJ, Anders A, Brown IG, Faehl RJ, Malik SM, Munson CP. Fundamentals of plasma immersion ion implantation and deposition. In: Anders A, editor. Handbook of Plasma Immersion Ion Implantation. New York: Wiley; 2000. p 243–302.
31. Tian XB, Kwok DTK, Chu PK. Modeling of incident particle energy distribution in plasma immersion ion implantation. J Appl Phys 2000;88:4961–4966.
32. Tan L, Dodd RA, Crone WC. Corrosion and wear-corrosion behavior of NiTi modified by plasma source ion implantation. Biomaterials 2003;24:3931–3939.
33. Green SM, Grant DM, Wood JV. XPS characterization of surface modified NiTi shape memory alloy. Mater Sci Eng A 1997;224:21–26.
34. Shevchenko N, Pham MT, Maitz MF. Studies of surface modified NiTi alloy. Appl Surf Sci 2004;235:126–131.
35. Chu PK, Tang BY, Cheng YC, Ko PK. Principles and characteristics of a new generation plasma immersion ion implanter. Rev Sci Instrum 1997;68:1866–1874.
36. Chu PK, Tang BY, Wang LP, Wang XF, Wang SY, Huang N. Third-generation plasma immersion ion implanter for biomedical materials and research. Rev Sci Instrum 2001;72:1660–1665.
37. Tadic D, Beckmann F, Donath T, Epple M. Comparison of different methods for the preparation of porous bone substitution materials and structural investigations by synchrotron MU-computer tomography. Materialwiss Werkst 2004;35:240–244.
38. Moulder JF, Stickle WF, Sobol PE, Bomben KD, Chastain J. Handbook of X-ray Photoelectron Spectroscopy: A Reference Book of Standard Spectra for Identification and Interpretation of XPS Data. Minnesota: Physical Electronics Division, Perkin-Elmer; 1992. p 72,73; p84, 85.
39. Wolff M, Schultze JW, Strehblow H-H. Low-energy implantation and sputtering of TiO_2 by nitrogen and argon and the electrochemical reoxidation. Surf Interface Anal 1991;17:726–736.
40. Tietze H, Mullner M, Selgert P. Temperature-induced precipitations in the memory alloy NiTi. J Phys D: Appl Phys 1984; 17:1391–1398.
41. Chu PK, Chan C. Applications of plasma immersion ion implantation in microelectronics—A brief review. Surf Coat Technol 2001;136:151–156.